Regular Article

Salinity stress-mediated lipid droplet production and liquid–liquid phase separation in Chlamydomonas reinhardtii

Shubhangi Pandey[1], Priyal Visavadiya[1], Vaidehi Patil[1], Janvi Jain[1], G. Archana[1,a], and Debjani Bagchi[2,b]

[1] Department of Microbiology and Biotechnology Centre, Faculty of Science, The Maharaja Sayajirao University of Baroda, Vadodara, Gujarat, India
[2] Department of Physics, Faculty of Science, The Maharaja Sayajirao University of Baroda, Vadodara, Gujarat, India

Abstract High salt concentrations cause osmotic shock and oxidative imbalance in microalgal cells, thereby causing cell death. Innovative strategies are required to overcome the survival barrier and enhance the net productivity of bioenergy feedstock like lipids. In the current study, a gradient strategy for salt addition was employed to cultivate *Chlamydomonas reinhardtii*, and the effect of the step size was analyzed. The highest production of lipids was obtained at 150 mM NaCl salinity stress from gradient cultivation methods. The single stage produces smaller sized lipid droplets while the gradient induces the assembly of larger droplets. Lipid droplet (LD) assembly was found to lead to liquid–liquid phase separation (LLPS) of LDs from the cytosol. The characteristic of LLPS was analyzed with the help of various parameters such as spatial separation of LDs, LD number and size, and the area fraction occupied by LDs, and observed to be dependent on the mode of cultivation and age of the culture. The fluctuations in LD number and area are quantified by the parameter α (a function of the variance) and observed to be high in salinity stress conditions, implying heterogeneous response to stress. The pathways associated with lipid production were analyzed with the help of gene expression changes, which regulate the synthesis and breakdown of lipids, influencing LLPS. The combined action of autophagy, de novo lipid synthesis, and starch degradation together were found to enhance the lipid production in the gradient method.

1 Introduction

In microalgae, lipid droplets are produced plentifully in response to external biotic and abiotic stresses during their growth. These are mainly composed of neutral lipids such as triacylglycerols, enveloped in a phospholipid monolayer. They play an important role in energy storage during stress, lipid metabolism, or as sites of different biochemical reactions. Moreover, the biodiesel produced by transesterification of triacylglycerols (TAG) harvested from lipid droplets form the third-generation source of biofuel. Salt stress is a well-studied cultivation environment to enhance the biofuel potential of microalgae [1]. Marine microalgal strain, *Chlamydomonas* sp. JSC4 generated high lipid content under nitrogen-depleting hypersaline conditions [2]. *C. reinhardtii* has been observed to have a dramatic increase in the fatty acid content in the presence of different salts such as NaCl, KCl, and LiCl [3].

Although lipid droplets are present in the microalgal cells even in the absence of stresses in normal photoautotrophic growth, they are less numerous and very small. The homogeneous state in which lipids are mixed in the cytosol is entropically favorable, but different growth conditions affect interactions or affinity that govern assembly and those that govern solubility, lead to multiple phase-separated states with minimized free energy. Especially in stressful growth conditions, lipid productivity is high and when the interactions between the lipids are energetically favorable, it leads to phase-separated lipid droplets, despite the entropic cost arising due to a more ordered state. This results in liquid–liquid phase separation with lipid-rich droplets in the cytosol matrix, with equal chemical potential maintained between both phases, eliminating net diffusive flux between the phases. Studies have shown

[a] e-mail: archanagayatri@yahoo.com (corresponding author)
[b] e-mail: debjani.bagchi@gmail.com (corresponding author)

that liquid–liquid phase separation of lipid droplets (LD) is involved in maintaining cellular redox levels [4]. Liquid–liquid phase separation is also a well-known phenomenon involved in regulating lipid droplet formation under stress [5]. In fact, LD formation acts as a buffer to protect the cell from free fatty acid toxicity during stress [6].

LDs are stabilized in the cytosol due to the presence of a phospholipid monolayer at the interface, which decreases the interfacial surface tension and enhances the bending rigidity [7–9]. Despite the acquired metastability, LDs are dynamic structures, and can increase in size due to Ostwald ripening and droplet coalescence [10]. Lipids like triacylglycerols have minimal solubility in aqueous media and hence have decreased Ostwald ripening processes. Droplet coalescence initiates with the development of a transient pore formation between the coalescing droplets spatially close to each other, eventually leading to the complete fusion of the droplets [9, 10]. The pore formation depends on the elasticity of the phospholipid monolayer at the interface, as the bending rigidity of this layer defines the energy cost required to deform this surface, which can be quantified by the line tension, Γ. The thermal fluctuations also drive the transient pore formation, and droplet coalescence occurs if the energy barrier given by Γ^2/γ is overcome. If surface tension γ is high and line tension, Γ is low, the energy barrier is less, then droplet coalescence becomes more probable [11]. Hence, the lipid droplets present a dynamically changing scenario and depend on the lipid turnover, droplet concentration fluctuations, enhanced lipid synthesis, and droplet growth by Oswald ripening and/or fusion [12]. It would be interesting to study the droplet growth dynamics in microalgae when exposed to salt stress, especially since optimizations are necessary for selecting the perfect condition for maximizing biofuel potential.

When using salinity stress for biofuel production in microalgae, an important aspect which should be considered is that salt stress has detrimental effects and results in the loss of lipid productivity due to cell death and poor biomass [1]. Two-stage cultivation has been found to cause biomass accumulation in the first stage, followed by exposure to stress elements in the second stage. This was observed to increase the net lipid content in microalgae [13]. Two-stage salt stress in *Chlamydomonas* sp. JSC4 has been observed to increase biomass accumulation and lipid content by nearly four times compared to single-stage [2]. In *Scenedesmus* sp. CCNM 1077, supplementing 400 mM NaCl in the second stage is observed to reduce the detrimental effects of stress and increases the production of biomass, chlorophylls, and carotenoids by as high as three times compared to single-stage cultivation [14]. A significant increase in lipid content by 2.5 times was also observed in *Chlorella vulgaris* when 500 mM NaCl was added with a two-stage strategy [15]. Recently, an advanced approach has evolved where stress elements are introduced in a stepwise/gradient strategy to induce gradual adaptation to stress [2, 16] experimented with marine microalga, *Chlamydomonas* sp. JSC4 using salt stress combined with nitrogen depletion. The authors observed maximum lipid content and lipid productivity in the case of salinity gradient. In a separate study, salinity-gradient in *Chlamydomonas* sp. JSC4 also resulted in enhanced biomass and lutein production [17]. Salinity gradient in other microalgae also results in improved biofuel potential [18, 19]. However, the possible alterations in the microalgal morphology and the metabolic pathways responsible for the enhanced biofuel potential in two-stage and salinity-gradient cultivation remains to be identified. Moreover, how morphology of the lipid droplets is affected due to LLPS under different growth conditions and the subsequent phase diagram has still not been explored.

In this study, the effect of NaCl at different concentrations applied in single-stage, two-stage, and gradient to *C. reinhardtii* (CC-125 strain) is studied. The production of lipids is studied as the function of culture age and growth phase. Single-cell fluorescence microscopy is performed to study the lipid droplet distribution and the morphological changes induced upon exposure to salt stress in different modes of cultivation. This study uncovers the involvement of liquid–liquid phase separation in lipid droplet formation in microalgae exposed to salt stress. The growth conditions, as well as culture age are observed to influence the phase coexistence boundary. Using qRT-PCR, the role of genes involved in autophagy, starch-to-lipid switching, and de novo lipid synthesis was investigated in two-stage and gradient modes of cultivation. Interestingly, bifurcated distribution of functions was observed in single stage versus gradient. Difference in gene expression profiles was observed to affect the lipid production, thereby modifying the forces driving LLPS. Hence, growth conditions are observed to greatly influence TAG and phospholipid productivity, lipid droplet size, morphology, and lipid–lipid interactions.

2 Materials and methods

2.1 Growth and maintenance of C. reinhardtii CC-125

Chlamydomonas reinhardtii CC-125 used throughout this study was procured from Chlamydomonas Resource Centre, Minnesota, USA. Microalgal cells were grown and maintained on Tris–acetate-phosphate (TAP) medium pH 7.0, containing 40 μg/mL ampicillin. The culture was grown at 25 °C with constant shaking at 200 rpm, and white light of ˜ 50 μmol photons/m s was provided maintaining a light:dark cycle of 12 h:12 h light.
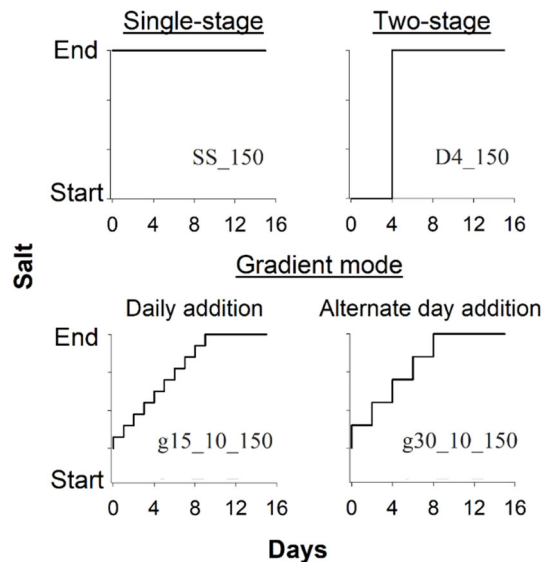
Fig. 1 A schematic representation of single-stage, two-stage, and gradient strategy of cultivation in the presence of 150 mM NaCl. Here, SS_150 means 150 mM NaCl added at the time of inoculation; D4_150 means the 150 mM NaCl is added on the 4th day of cultivation. g15_10_150 has 15 mM NaCl, added daily for up to 10 days of growth. The step size here is 1 day. g30_10_150 has doubled the NaCl concentration, i.e., 30 mM, added on alternate days up to the 10th day of growth. The step size, thus, is 2 days in this case

2.2 Cultivation strategies of C. reinhardtii under salt stress

Salt stress was provided using sodium chloride (NaCl) at 150 mM concentration as 100 mM showed less lipid productivity and 200 mM was observed to severely compromise the growth (data not shown). In the single-stage mode of cultivation designated as SS_150, salt was added at the commencement of cultivation. In the two-stage designated as Dx_150, salt was added on the xth day of growth. In this study, $x = 2$ or 4, i.e., in the log phase of the culture. In the gradient mode of cultivation, a known concentration of salt is added stepwise at fixed time intervals to achieve the final concentration. Gradient strategy is categorized into two types: g15_10_150 has 15 mM added daily, respectively, up to 10 days of growth, while g30_10_150 has doubled the NaCl concentration, i.e., 30 mM added on alternate days up to 10th day of growth. Thus, the final concentration in both cases is attained at the same time of growth but in varying step sizes, it is 1 day in the first case and 2 days in the latter. The schematic representation of salt stress delivered for the final concentration of 150 mM is illustrated in Fig. 1.

2.3 Cell count using a haemocytometer

To avoid redundancy in counting, *Chlamydomonas* cells were first immobilized by providing a 10 min cold shock treatment to the liquid culture The cell count present in a given volume of culture at different growth stages with known absorbance at 680 nm (OD_{680}) was obtained using a haemocytometer and a linear graph between OD_{680} (measured using a UV–visible spectrophotometer UV-1800, Shimadzu) and the cell count was plotted. An equation correlating cell density and OD_{680} was derived from the linear fit using OriginPro 9.0 software. This equation was used to calculate the cell density directly from measured OD_{680} values.

2.4 Estimation of neutral lipid content using Nile red dye

The neutral lipids synthesized by microalgae under stress are stored in the form of triacylglycerols (TAG) enclosed in lipid droplets (LD). LDs were stained using Nile red dye (Sigma-Aldrich Pvt. Ltd). The CC-125 cells were incubated for 10–15 min at 25–28 °C in dark with Nile red dye solution in DMSO at a final concentration of 1 µg/mL [20, 21]. Nile red forms a complex with TAG molecule whose fluorescence was captured using a filter set with $\lambda_{ex} = 485 \pm 20$ nm and $\lambda_{em} = 590 \pm 35$ nm in a multi-mode microplate reader (BioTek Synergy HT, now called Agilent). The final TAG concentration was calculated in fluorescence units (f.u.) per mL and f.u. per 10^6 cells after normalizing the readings with the experimental controls.

2.5 Epifluorescence live-cell imaging of lipid droplets

Lipid droplets were stained with 1 μg/mL Nile red dye. Post-staining, cells were observed with Olympus BX53F2 upright optical microscope in epifluorescence mode, using a 130 W U-HGLGPS excitation source, TRITC filter, and $100\times$ (1.4 NA) Olympus oil-immersion objective. In all the measurements, ~ 100 cells were imaged with an Olympus DP74 camera. An autotrophic control with no stress exposure was also recorded for reference. Images were processed using Image J software (Fiji). Briefly, individual cells were selected and analyzed for the total fluorescence intensity of a cell (pixels), size of the lipid droplets (μm^2) contained in a cell, size of the cell (μm^2), and fluorescence intensity of the lipid droplets occupying the cell (pixels), using a custom-made program. The percent area of the cell occupied by lipid droplets (φ) was calculated for LLPS analysis. As a control to test specificity of Nile red binding to lipid droplets, high-resolution images were also obtained with a confocal microscope (Olympus, with 488 nm laser excitation and 590 nm emission, using UPLSAPO $100\times$ oil-immersion objective, NA = 1.4).

2.6 Statistical analysis

The reported values were derived from an average of three independent biological replicates, and the errors represent the standard deviation (S.D.). Statistical significance of the data was obtained by Student's t-test analysis performed in MS Excel, where the data were considered significant only if $p \leq 0.05$. The maximum significance of the data was obtained with $p \leq 0.0001$.

## 2.7 Total RNA extraction and quantitative real-time PCR

The RNA extraction was done using the TRI Reagent from Sigma as described previously by Bell et al. [22]. Here, ~ 5×10^6 *Chlamydomonas* cells were homogeneously mixed in TRI Reagent and the mixture was subsequently treated with chloroform. The total RNA extracted in the aqueous layer was then precipitated by isopropanol, and the precipitated RNA pellet was washed with chilled 70% ethanol. The isolated RNA was treated with DNase I (final concentration, 1 U) at 37 °C for 40 min and the total RNA was quantified. A total of ~ 1 μg of RNA was converted to cDNA using Anchored Oligo dT primers from Verso cDNA synthesis kit, ThermoFisher Scientific. The reaction for qPCR contained ~ 6 ng of cDNA sample along with TB Green Premix Ex Taq II (Tli RNase H Plus) from Takara Bio, and a gene expression study was performed on the Applied Biosystems StepOne Real-Time PCR system. Gene-specific primer pairs were designed using Primer 3 software as follows: *ACC*: 5′-CATCATCTCGGTGGTCATTG-3′ and 5′-GCGTTCTCCATGATCAGGTT-3′; *ATG4*: 5′-ACTGGGCATGGACAAGATCA-3′ and 5′-TCGAGGTAGATGAAGGACGC-3′; *ATG8*: 5′-CGCATCAAGGAGAAGTACCC-3′ and 5′-TGCGGATGACGTACACAAAT-3′; *PhoA*: 5′-TACCTGCGCCTGTACTTCCT-3′ and 5'-GATCAGGCAACCGTTCATCT-3′; *DGAT*: 5′-CCAAGGTGGCTCGTGACTC-3′ and 5′-ACTCGCCTCTGTGCCTGTT-3′; *RPS6*: 5′-TACGTCAiCCATCTACTCGCG-3′ and 5′-GCGTCGGTCTTGTTCTTCTC-3′; and *RACK1*: 5'-TCAACATCACCAGCAAGAAGG-3′ and 5′-CTGGGCATTTACAGGGAGTG-3′. *RACK1* was used as a housekeeping gene and primers for *DGAT* and *RACK1* were used as already reported [23]. All the experiments were performed in triplicates to check reproducibility.

3 Results

3.1 Growth and biomass production in C. reinhardtii under salt stress

Chlamydomonas reinhardtii CC-125 grown under optimum conditions in the present laboratory setup has the logarithmic phase of growth lasting for 4 days after which it enters the stationary growth phase. The cultures were monitored for 15 days of growth. We initiated the study with low salt concentration and explored the variations under two-stage cultivation only. The addition of 100 mM NaCl showed no significant change in the growth profile. Figure 2A depicts the effect of 150 mM salt concentration on the growth of *C. reinhardtii*, where we introduced the gradient strategy of cultivation. Two different step sizes were used, salt added at an interval of 1 day (g15_10_150) and salt added at an interval of 2 days (g30_10_150) (Fig. 2A). Cultures incubated with 150 mM NaCl, g30_10_150 (step size of 2 days) showed the highest biomass accumulation of 4.67 ± 0.75 million cells/ml on the 15th day. On the other hand, g15_10_150 (step size of 1 day) and SS_150 were the most adversely affected conditions. Thus, the gradient mode of cultivation improved cell growth over the two-stage mode of cultivation which was even better than the single-stage at 150 mM NaCl. Overall, g30_10_150 yields the maximum biomass among all the salt stress conditions (Fig. 2A).

Fig. 2 The density of *C. reinhardtii* CC-125 cells and TAG production in the presence of 150 mM NaCl. **A** The cell density in the presence of 150 mM NaCl. Here, "**SS**" stands for single-stage, and "**D4**" means two-stage where NaCl was added on the 4th day of growth. **g15_10_150** has 150 mM NaCl, added daily up to 10 days of growth, while **g30_10_150** has doubled the NaCl concentration, i.e., 30 mM, added on alternate days up to 10th day of growth. The error bars represent the standard deviation derived from the three independent biological replicates. **B**, **C** The TAG content in f.u. per million cells and ml, respectively. Error bars represent standard deviation for $n = 3$. *$p \leq 0.5$, **$p \leq 0.01$, ***$p \leq 0.001$, ****$p \leq 0.0001$
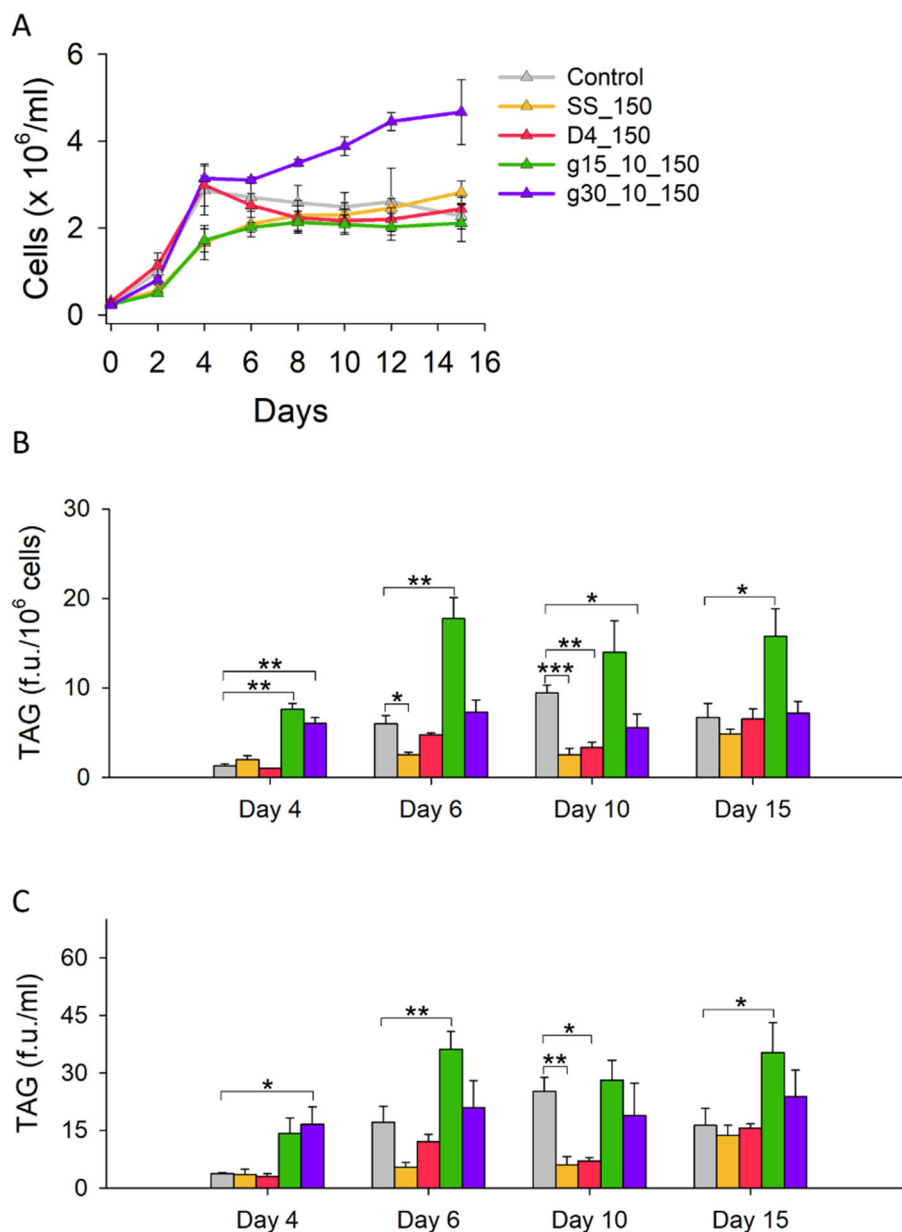
3.2 Lipid production in C. reinhardtii under salt stress

To study lipid production, the *C. reinhardtii* cells were stained with Nile red after making them permeable with DMSO. Nile red stains neutral lipids effectively, and fluorescently stained lipid droplets in about ~ 100 cells were imaged with an epifluorescence microscope. The average fluorescence intensity observed in all the cells was calculated (Fig. 2B, C). Examination of 150 mM stress condition showed that the maximum starch content is obtained on day 4 in 150 mM NaCl. TAG content reaches the maximum on day 6 in the presence of 150 mM NaCl. TAG production was observed to be compromised in SS_150 and significantly higher in g15_10_150. Despite poor cell density in g15_10_150, it yields the maximum TAG of 36.18 ± 4.6 units/ml on day 6. Hence, the study illustrates that the mode of cultivation is a key factor in diverting the metabolite production pathway from starch to lipid or vice versa. The stress response is dose-dependent, and 100 mM NaCl showed no effects of stress on the microalgal cells, while 200 mM NaCl showed lethal effects (data not shown). In the present study, 150 mM NaCl seems to yield the highest biomass and lipid content. The gradient cultivation strategy helps in building biomass better than the two-stage strategy.

3.3 Morphological changes in C. reinhardtii cells under 150 mM NaCl stress

Figure 3a shows representative epifluorescence images of cells stained with Nile red for all culture conditions at Day 10. Higher resolution Nile red fluorescence confocal microscopy images are also shown for the Control culture in Fig. 3b, to illustrate the binding specificity of Nile red to lipid droplets and the absence of pigment fluorescence from the cup-shaped chloroplast. The two very prominent features, i.e., palmelloid formation (organization of cells into a multicellular structure, having a single cell wall and polysaccharide gel in between to combat environmental stress) and loss of photosynthetic pigments, were noticed as a function of changing modes of cultivation (Supplementary Fig. 1). First, a thick layer of palmelloid sheet was observed in SS_150 condition, otherwise very thin in two-stage and gradient cultivations. This was accompanied by the high-order organizations of cells in single-stage since day 6. The strength of the organization went up to as high as 8 cells on day 10 in SS_150, while it was only 4 cells in two-stage and gradient. Second, the pigment content was impaired in D4_150 day 6 onwards. This loss of pigments can also be observed in SS_150 and g30_10_150 on day 10. Since the lipid droplets were found to be majorly distributed in the cytosolic area of the cell, this distribution spreads to the entire cellular area in bleached cells. The cell size distribution (Fig. 4) suggests that the cell size decreases in SS_150, D4_150, and g15_10_150 from day 4 to day 10, while it increases in Control and g30_10_150. The cell size, as compared to the Control, is drastically reduced in single-stage and gradient cultivations on day 6 and under all salt stress conditions on day 10. Thus, effects of osmotic shock are also observed for stepwise increment of salt concentration in *C. reinhardtii* cells, with reduction in the cell size. However, the cell size in the g30_10_150 condition is larger than SS_150 on day 10. This suggests that the step size of salt addition is an important factor in controlling the osmotic pressure on the cell. We also studied the distribution of the cell circularity in the population of microalgal cells under salt stress (Fig. 5). There was no significant difference in the cell shape across the population of stress-exposed cells as compared to the Control, except for the appearance of bimodal distribution in SS_150 on day 4, with a small sub-population having distorted circularity. Sudden exposure to high salt concentration led to the immediate disturbance in cell membrane integrity which got optimized later with time.

Further, the distributions of the average size of lipid droplets produced by the microalgal cells in the presence of 150 mM NaCl (Fig. 6) revealed interesting features of lipid droplets as a function of mode of salt stress. Huge droplets were observed in SS_150 on day 4. However, their size began to decrease with age. In contrast, the droplet size in g15_10_150 was observed to increase with time. Overall, both SS_150 and g15_10_150 cultivations led to the formation of large lipid droplets but at different timelines. The droplet size in g30_10_150 peaked on day 6.
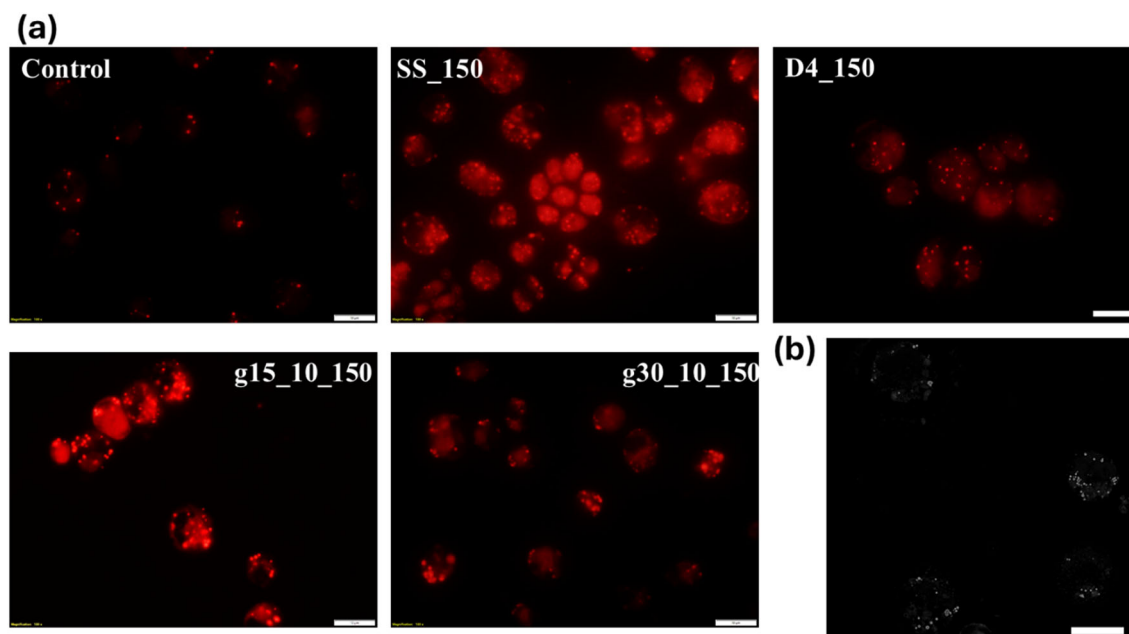

Fig. 3 a Nile red epifluorescence microscopy images of *C. reinhardtii* observed with 100×, grown under different conditions as labeled, at Day 10. To maintain a constant intensity scale over all conditions, the images are normalized with the help of gamma correction, a non-linear histogram adjustment given by the equation New intensity $= 255 \times \left[(\text{old intensity}/255)^{1/\gamma} \right]$, with $\gamma = 2$ for all images; the maximum intensity is 255 and the minimum intensity 0. **b** Representative Nile red-stained confocal microscope image of the cells of the Control culture. All scale bars represent 10 µm
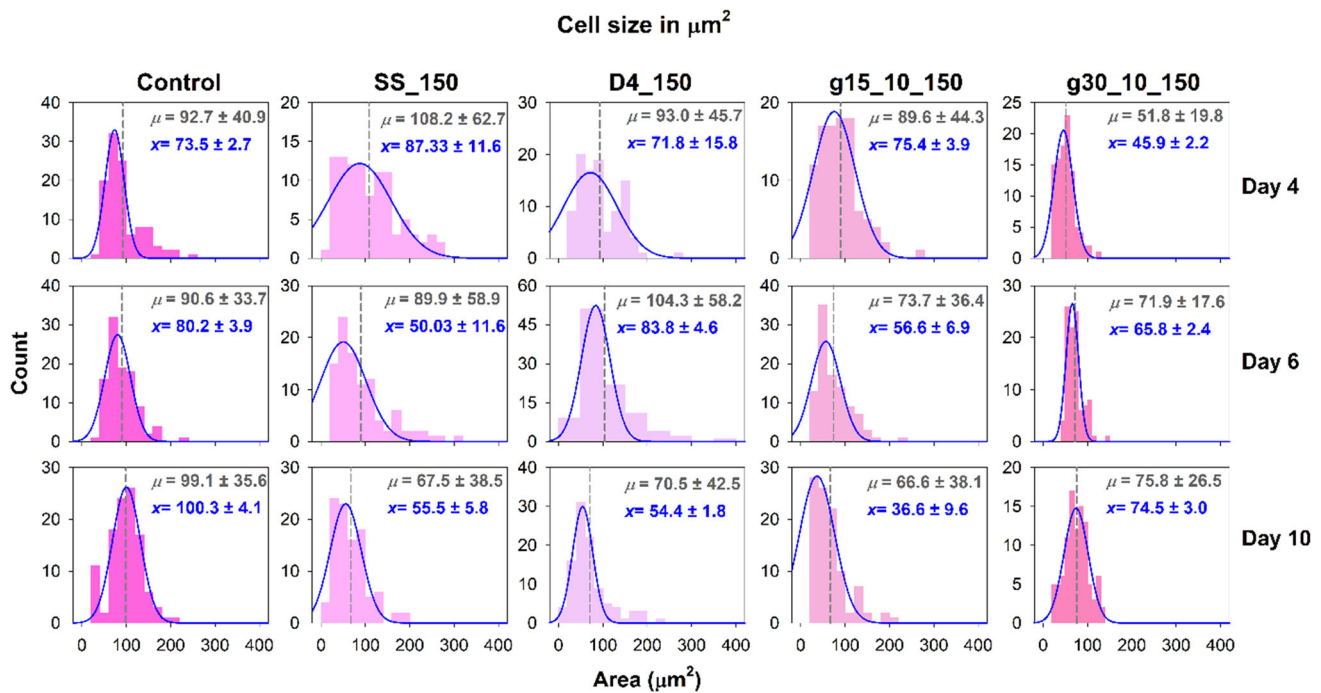
Cell size in μm²

Fig. 4 Probability distribution of the size of *C. reinhardtii* cells when grown in the presence of 150 mM NaCl. Pink-shaded bars represent the histogram of the size of ˜ 100 cells in terms of the area (μm²), the grey-colored dashed vertical lines in each graph represent the population mean μ, blue-colored graphs represent the normal distribution fit of the histograms and x is the mean obtained from the fit
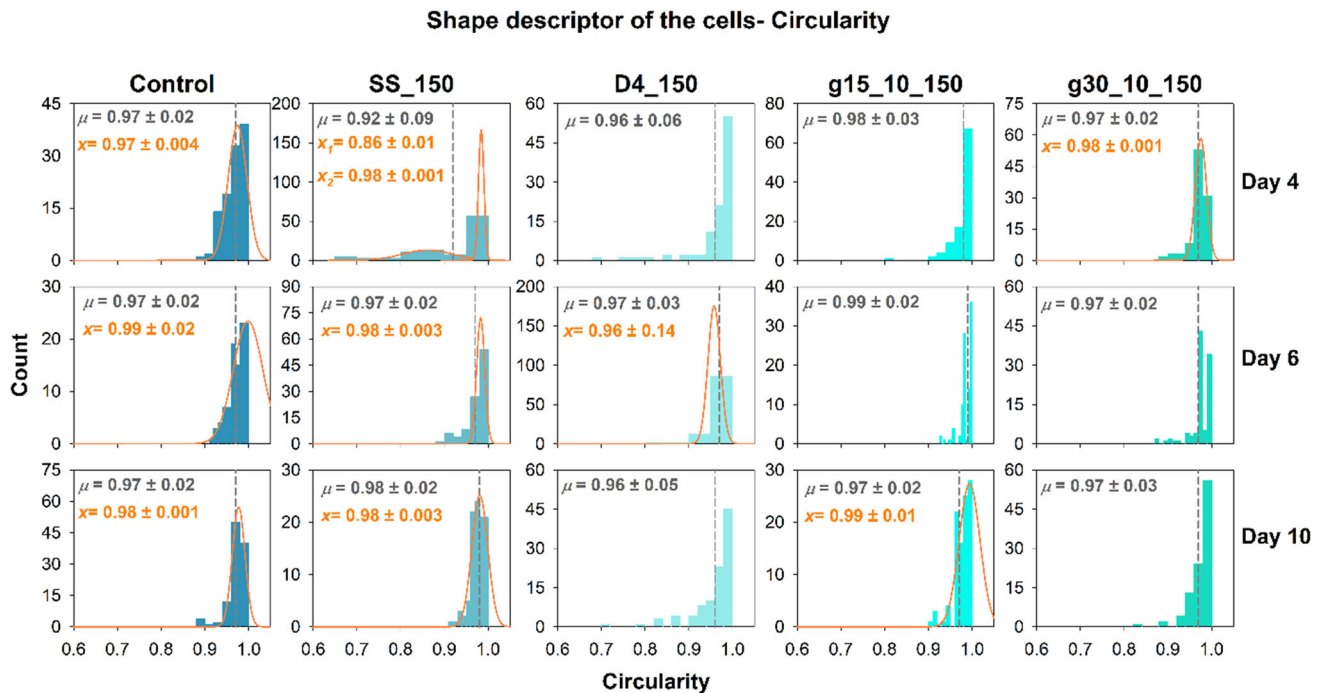
Shape descriptor of the cells- Circularity

Fig. 5 Probability distribution of the shape of *C. reinhardtii* cells when grown in the presence of 150 mM NaCl. Cyan-shaded bars represent the histogram of the shape of ˜ 100 cells in terms of circularity, grey-colored dashed vertical lines in each graph represent the population mean μ, orange-colored graphs represent the normal distribution fit of the histograms and x is the mean obtained from the fit
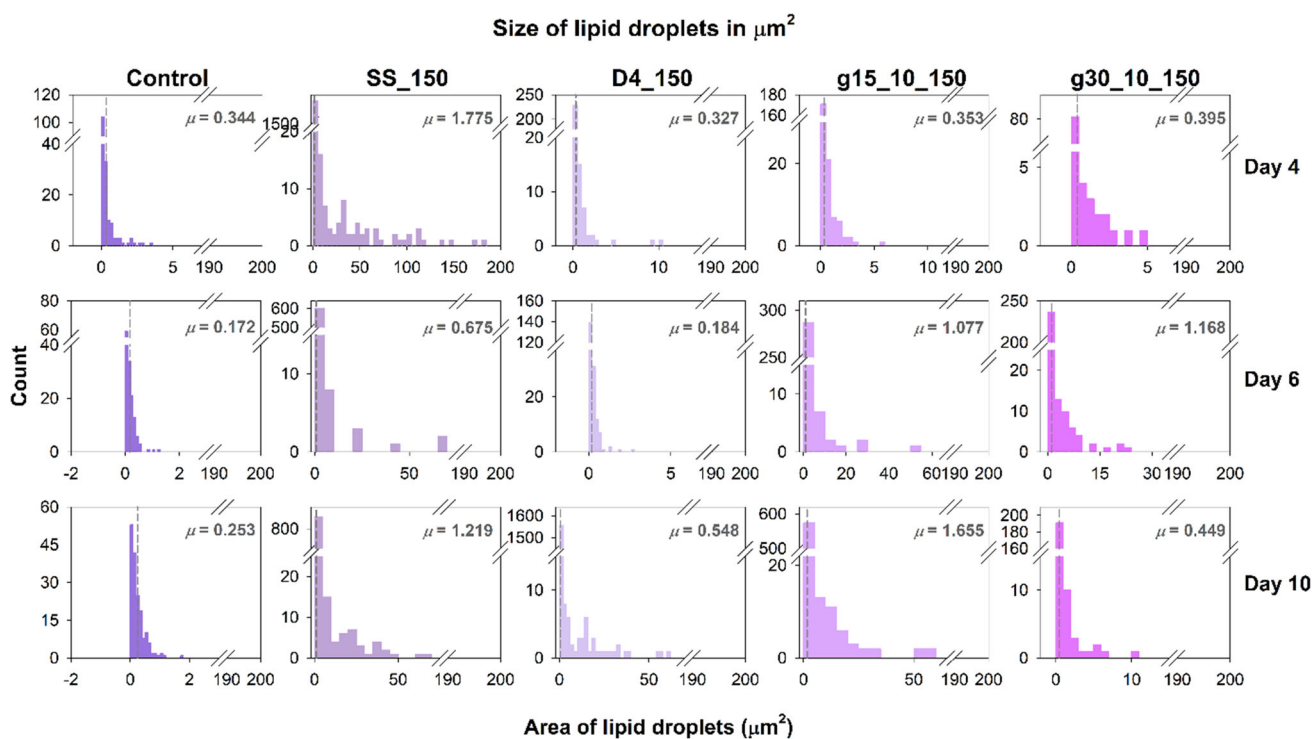
Fig. 6 Probability distribution of the size of lipid droplets produced by *C. reinhardtii* in the presence of 150 mM NaCl. Purple-shaded bars represent the histogram of the size of lipid droplets produced by ˜ 100 cells in terms of the area (μm^2), and grey-colored dashed vertical lines in each graph represent the population mean μ. Since the histograms are not normally distributed, they could not be fitted

D4_150 caused a significant size reduction in their lipid droplet formation. These results suggest that the mode of cultivation plays an important role in governing the size of lipid droplet formation. The smallest change in the step size of salt addition also triggers significant changes in droplet synthesis. It would be interesting to study the physical factors associated with the droplet distribution inside the cell as the function of the mode of cultivation in *C. reinhardtii* under salt stress.

3.4 Lipid droplet growth dynamics and phase behavior in C. reinhardtii in the presence of 150 mM NaCl

The coexistence of the hydrophobic lipid droplets in the hydrophilic cytosol is very interesting since the microscope images reveal reasonably stable droplet structures. Lipid droplet statistics such as the droplet count per area of the cell (Fig. 7) and the percentage area of the cell occupied by these droplets, φ (Fig. 8), were calculated for about 100 cells for each condition, and probability distributions were obtained, which gave the variation (standard deviation) as well as the average parameter analyzed. While the droplet count per area symbolizes the droplet density, the percent area occupied gives an idea of the coexistence ratio of droplets in 2D with respect to the cytosol inside the cell. Fluctuations in the number of droplets and percentage area occupied by the lipid droplets are quantified by the parameter, α ($\alpha = v/x^2$ where v is the variance in the data, and x is the mean of the variable) (Fig. 9), across a population of ˜ 100 cells for a particular culture condition. It should be noted that for data with similar variance, the ones having lower mean values would show higher α, and vice versa (as is the case for the Control culture on Day 6, on comparison of Figs. 7 and 9). High variability is observed in the salt stress conditions when compared to the Control culture. The maximum variability in number of lipid droplets is present in g15_10_150 on Day 4 and in SS_150 on Day 6 of growth for percentage area occupied by lipid droplets. The fluctuations confirm that the heterogeneous distribution in the data is not an experimental artifact and occur due to variable sub-populations in the culture, revealing heterogeneous cellular response in cells even within a single population. Further, an increased number of lipid droplets per area of the cell was observed in both SS_150 and g15_10_150, more prominently higher in the single stage (Fig. 7). Interestingly, it was the highest in D4_150 on day 10. Thus, D4_150 resulted in the production of small-sized droplets (Fig. 6), however more densely packed inside the cell. In contrast, g30_10_150 produced loosely packed but large-sized droplets (Fig. 6). Further, the area occupied by these droplets was also found to be highest in SS_150 on all days of growth, while g15_10_150 showed an increase in the area occupied by their droplets on days 6 and 10 only (Fig. 8). A considerably large area was occupied by
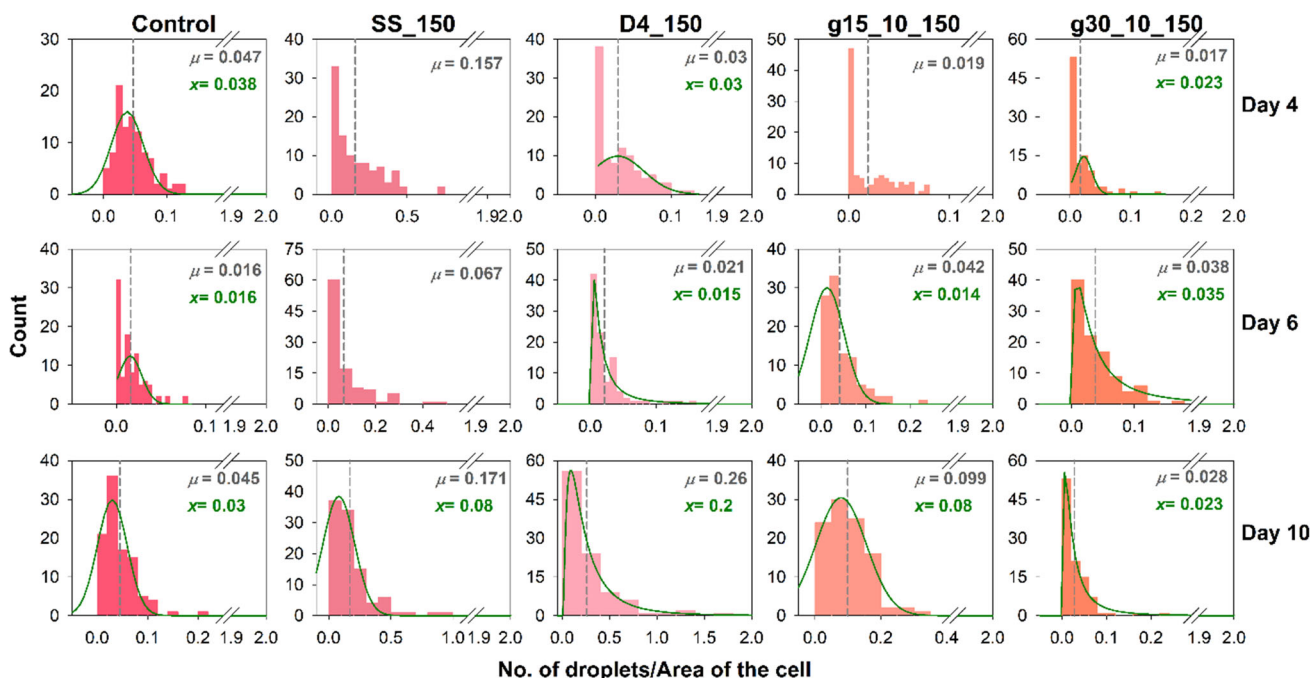
Fig. 7 Probability distribution of the number of lipid droplets distributed per area of the *C. reinhardtii* cell in the presence of 150 mM NaCl. Red-shaded bars represent the histogram of the size of lipid droplets produced by ˜ 100 cells in terms of the area (µm²), and grey-colored dashed vertical lines in each graph represent the population mean µ. The green-colored graphs represent the normal or log-normal distribution fits with mean x
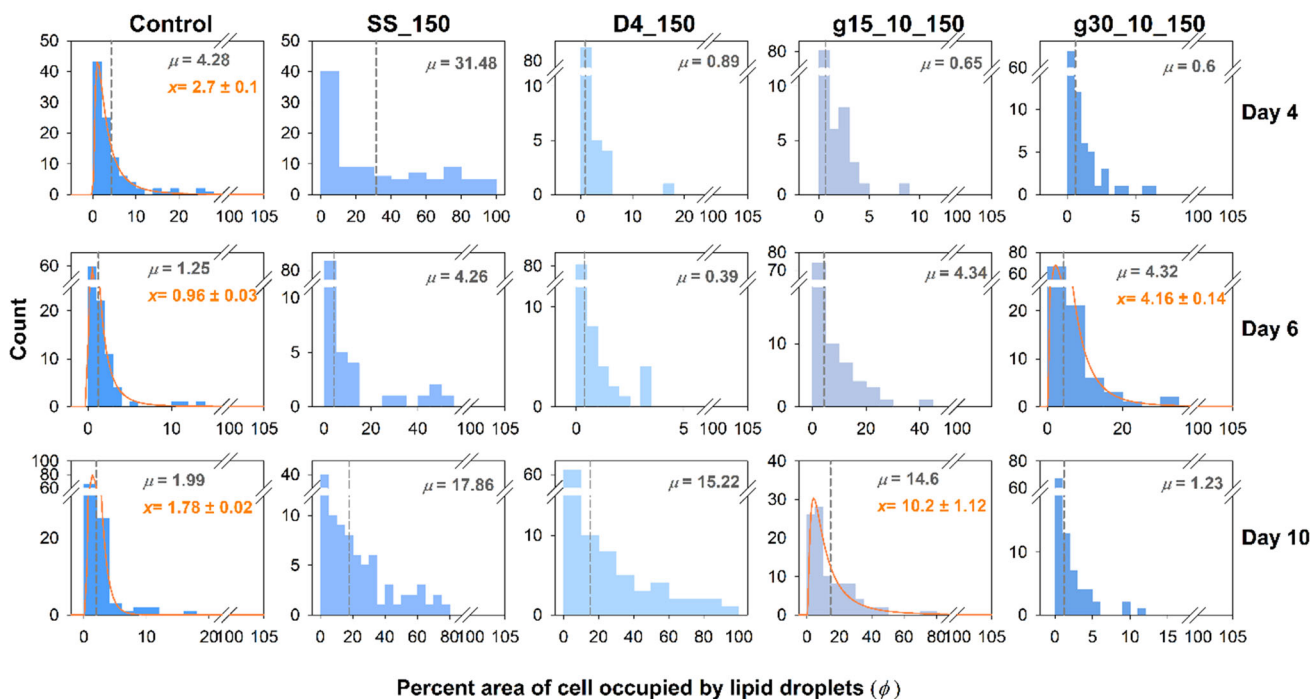

Fig. 8 Probability distribution of the percentage area of the cell occupied by the lipid droplets produced by *C. reinhardtii* in the presence of 150 mM NaCl. Blue-shaded bars represent the histogram of the size of lipid droplets produced by ˜ 100 cells in terms of the area (µm²), and grey-colored dashed vertical lines in each graph represent the population mean µ. The orange-colored graphs represent the log-normal distribution fits with mean x

Fig. 9 Fluctuations in the droplet growth dynamics in *C. reinhardtii* under the presence of 150 mM NaCl. Fluctuations (α) in the number of lipid droplets (**A**) and the percentage area occupied by lipid droplets per cell, φ (**B**), as a function of culture growth condition and age. Here, $\alpha = v/x^2$ where α is the fluctuation in the measured variable, v is the variance in the data, and x is the mean of the variable
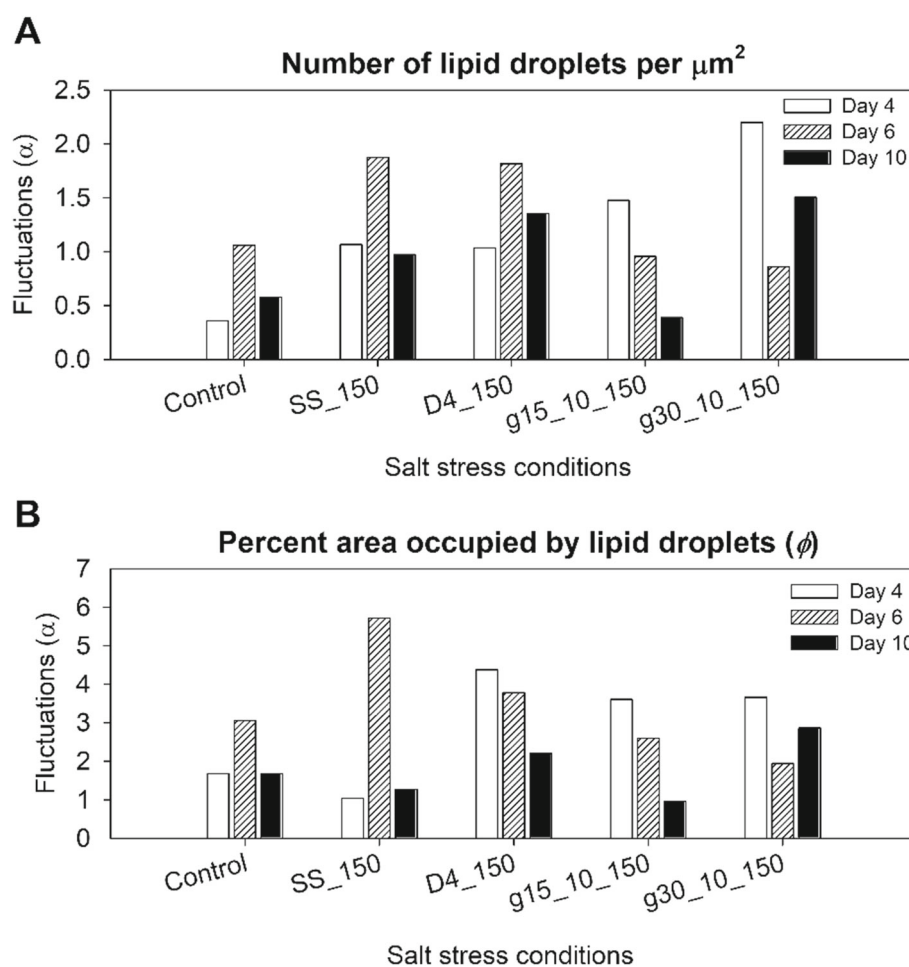
droplets in D4_150 on day 10 and g30_10_150 on day 6, suggesting a widespread distribution of droplets. Overall, the droplet distribution varies among different cultivation modes under salt stress.

The total number of droplets was segregated into three categories of different size ranges (as mentioned in the figure caption, Fig. 10). The spatial segregation of the lipid droplets in the cell based on their size showed a rich, salt-stress condition-dependent phase behavior. The maximum number of lipid droplets is observed in SS_150 on day 4 followed by D4_150 on day 10. After proportionating, it was found that this increase is mainly contributed by the small-sized droplets (Fig. 10B). Gradient cultivations result in a low count but a significantly higher proportion of larger lipid droplets (Fig. 10A). These results imply that single-stage and two-stage impose an increase in the number of smaller lipid droplets while gradient cultivation leads to synthesis of larger lipid droplets. The lipid droplets are usually found to be in the two-phase or phase-separated state in the cytosol, and different conditions yield different phase coexistence boundaries, as shown in Fig. 11 where the area fraction of droplets is plotted as a function of culture age. The shaded regions in this figure denote the two-phase state. The enhanced production of lipids, and increase in droplet size, as well as density, leads to droplets that completely encompass the cytosol, resembling a mixed, one-phase state. This one-phase state mostly commences towards the later part of the stationary growth phase or at the beginning of single-stage salt stress, absent otherwise in the Control culture. Thus, SS_150 possesses the highest amount of phase-separated lipid droplets at all phases of growth. Gradient, g15_10_150, shows an increasing population of phase-separated droplets along with the culture age. This can be explained by the increasing lipid concentration at the stationary phase (Fig. 2). The variable phase coexistence boundaries, as well as droplet size for the growth conditions studied, point at the presence of variable forces driving these phase transitions. In addition to lipid–lipid interactions governed by lipid composition, lipid turnover and lipid degradation mechanisms play an important role in influencing these forces. In all growth conditions, culture age is chosen as the field which influences the fraction of area occupied by lipid droplets (φ). Interestingly, in the phase coexistence curve of D4_150, there appears to be a reentrance of the one-phase (mixed phase) state just before Day 6 (Fig. 11). As this culture reaches stationary state in Day 10, there is an increase in the smallest sized detectable lipid droplets (Fig. 10 B). These droplets are the major contributors of the enhanced area fraction at Day 10 in D4_150 culture. In case of SS_150, since salinity stress is applied in the beginning of
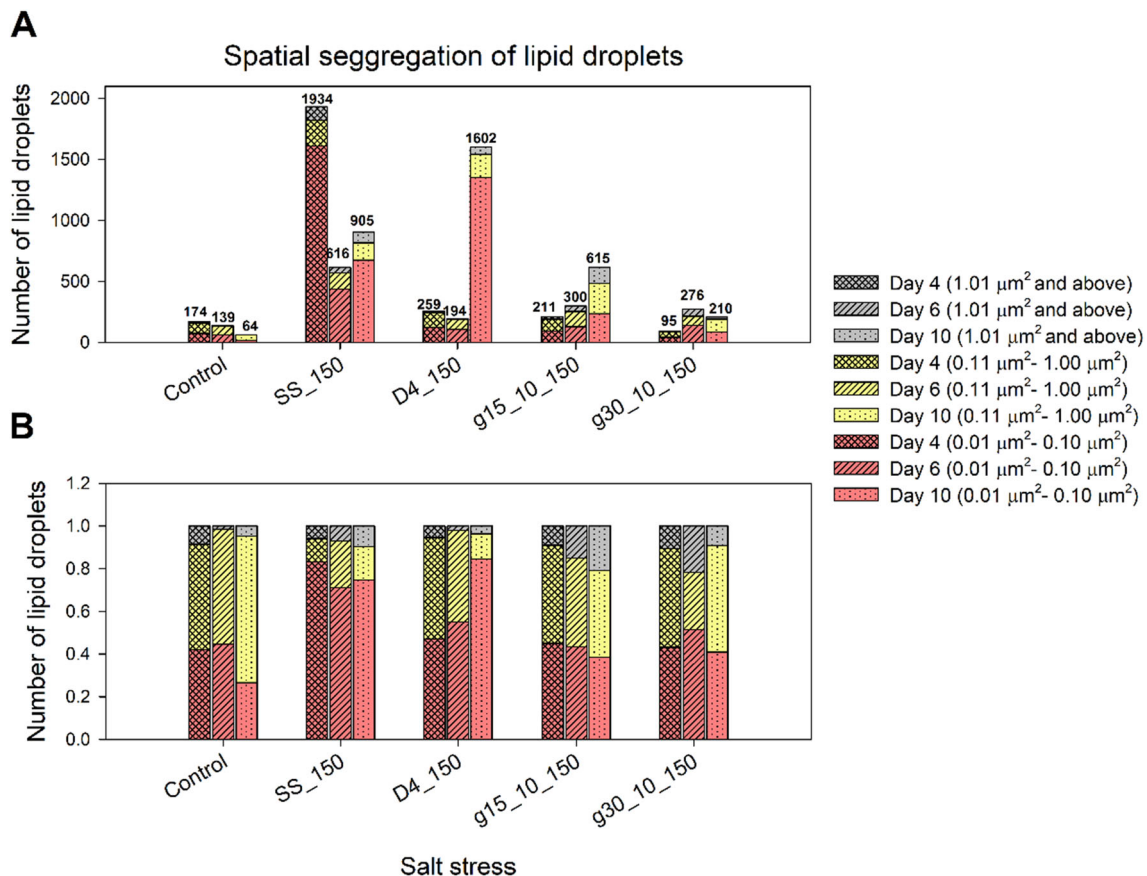
Fig. 10 Spatial segregation of lipid droplets in the *C. reinhardtii* cells observed under the presence of 150 mM NaCl. **A** Average number of lipid droplets per cell for different growth conditions, with each bar representing the culture age, for a particular growth condition. **B** Normalized bar plot representation of the number of droplets to show the fraction of each of the three categories of droplets in a cell for a given growth condition and culture age. The cross-checked bars represent day 4, bars with slants represent day 6 and dotted bars represent day 10. The droplets are subdivided into three categories based on their size—the largest droplets ($1.01 \ \mu m^2$ and above) are represented by gray-colored bars, the intermediate-sized droplets (0.11–$1.00 \ \mu m^2$) are shown in yellow color, and the smallest droplets (0.01–$0.1 \ \mu m^2$) are represented by the red shade

growth, the smallest-sized droplets are observed to be more numerous in Day 4 (Fig. 10 B), which are the largest contributors of the enhanced area fraction of the demixed state at Day 4 (Fig. 11) in SS_150. These features of lipid droplet distribution as measured by the single-cell 2D epifluorescence microscopy would have otherwise remained undetected and unexplored in the average bulk measurements.

3.5 Expression analysis of genes involved in growth, autophagy, and de novo lipid synthesis in C. reinhardtii

As observed previously, biomass and lipid yields were maximum in the presence of 150 mM NaCl along with a good yield of starch and pigments. Therefore, it would be interesting to analyze the expression levels of genes known to play a role in enhanced lipid accumulation under stress. A total of 6 genes were studied, involved particularly in starch degradation (*PhoA*), de novo lipid synthesis (*ACC* and *DGAT*), autophagy (*ATG4* and *ATG8*), and protein synthesis and autophagic flux (*RPS6*). The expression level of these genes in single-stage, two-stage, and gradient cultivations was studied in comparison to the housekeeping gene, *RACK1* on the 4th day (log phase) and 10th day (stationary phase) of the growth (Fig. 12). *ATG4* and *ATG8* are the autophagic genes responsible for coding AuTophaGy-related proteins, ATG4 and ATG8. Together, they assist in autophagosome formation induced by stress and result in the catabolic breakdown of membrane lipids, thereby increasing the carbon pool [24]. *RPS6* codes for ribosomal protein S6, a component of the smaller ribosomal subunit, which plays a vital role in cell growth and is an indicator of autophagic flux [24]. In this study, both *ATG4* and *ATG8* are highly upregulated in D4_150 and g15_10_150 on day 10. While *ATG4* in g15_10_150 is upregulated by 47.6-fold, *ATG8* is upregulated by 28.9-fold. D4_150 exhibits a 19.7-fold change in *ATG4* levels and a 161.8-fold change in *ATG8*.
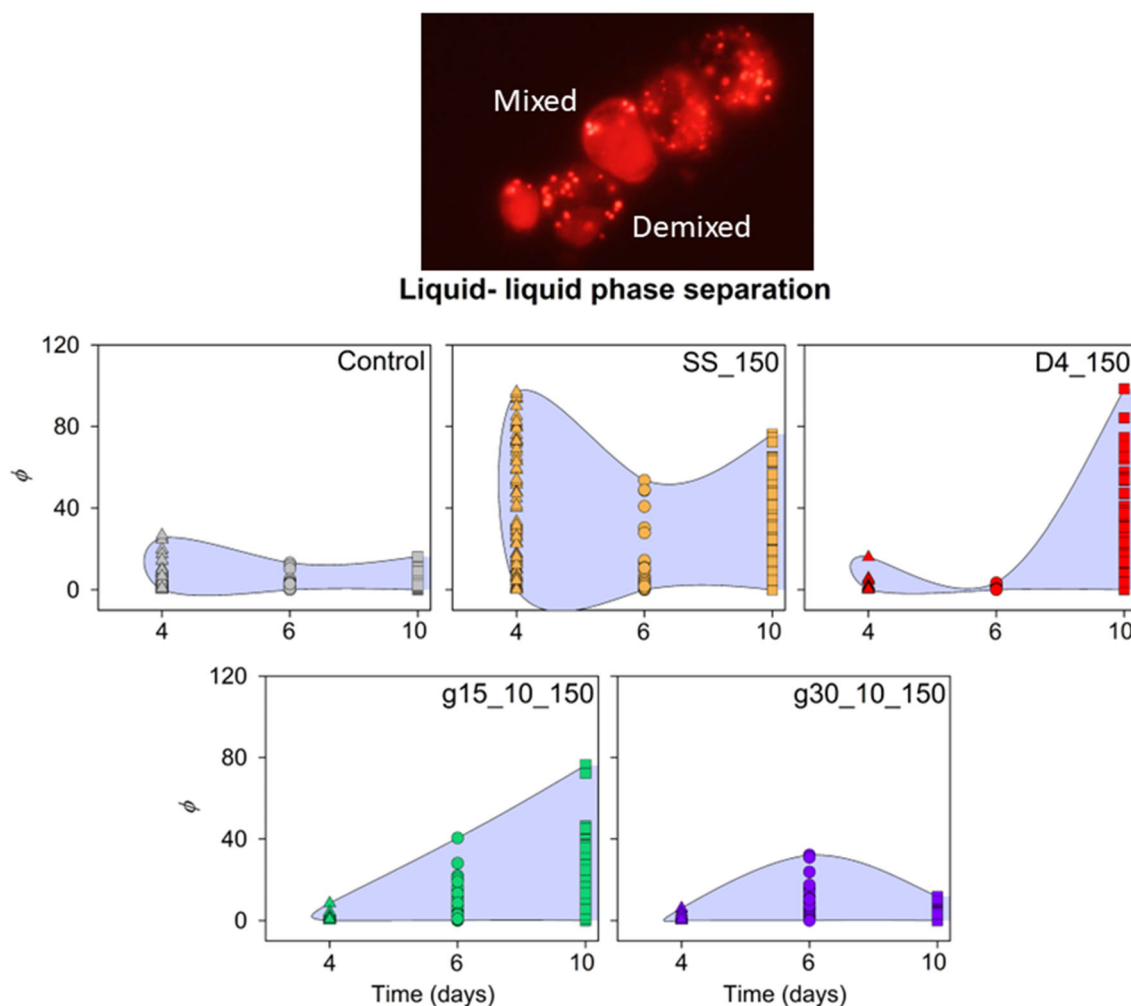
Fig. 11 Liquid–liquid phase separation in lipid droplet biogenesis in *C. reinhardtii* under the presence of 150 mM NaCl. Two-phase (demixed) coexistence boundaries, with the blue region representing lipid droplets coexistence with the cytosol, for different growth conditions of *C. reinhardtii*. The fraction of area occupied by lipid droplets (φ) as a function of the age of the culture is plotted as a function of time in days. The topmost panel illustrates the tendency of the lipid droplets (Nile red stained, red color) in *C. reinhardtii* cells to be in demixed or mixed state with the cytosol

RPS6 is upregulated in g30_10_150 on day 4 and D4_150 on day 10. However, D4_150 shows an upregulated expression of both *RPS6* and autophagy-related genes *ATG4* and *ATG8* on day 10. This suggests that two-stage cultivation induces autophagy without involving ribosomal protein turnover. Further studies might shed more light on the same. Besides D4_150, g15_10_150 shows a downregulated expression of *RPS6* and upregulation of both *ATG4* and *ATG8* on day 10, prominently pointing at the active autophagy in action.

g15_10_150 further shows highly upregulated levels of expression of *ACC*, *DGAT*, and *PhoA* on day 10. *DGAT* codes for the diacylglycerol acyltransferase (DGAT) enzyme which catalyzes the acylation of the DAG molecule to form TAG and represents the de novo TAG synthesis [25]. *ACC* encodes acetyl-CoA carboxylase, the rate-limiting enzyme which adds the carboxyl moiety to the acetate molecule [26]. After this step, the carboxy-acetylated molecule is fluxed into the de novo fatty acid synthesis pathway. *PhoA* encodes for starch phosphorylase A, which adds a phosphate group to the starch molecule. This leads to the degradation and formation of glucose-1-phosphate (the first step in lipid synthesis). Starch-to-lipid switching is a well-known phenomenon that aids in the lipid accumulation process under stress [27]. The current findings suggest a concerted action of de novo lipid synthesis, starch degradation, and autophagy regulating the enhanced lipid production (Fig. 2). Further, the increased levels of *ACC* by 125-fold in SS_150 on day 4 signify the involvement of de novo lipid synthesis in lipid accumulation in the single-stage cultivation.

Overall, single-stage cultivation features enhanced levels of de novo lipid production in the log phase of their growth. Two-stage cultivation induces autophagy without affecting protein turnover activity. The gradient cultivation strategy exhibits highly upregulated levels of autophagy, starch degradation, and de novo lipid production.
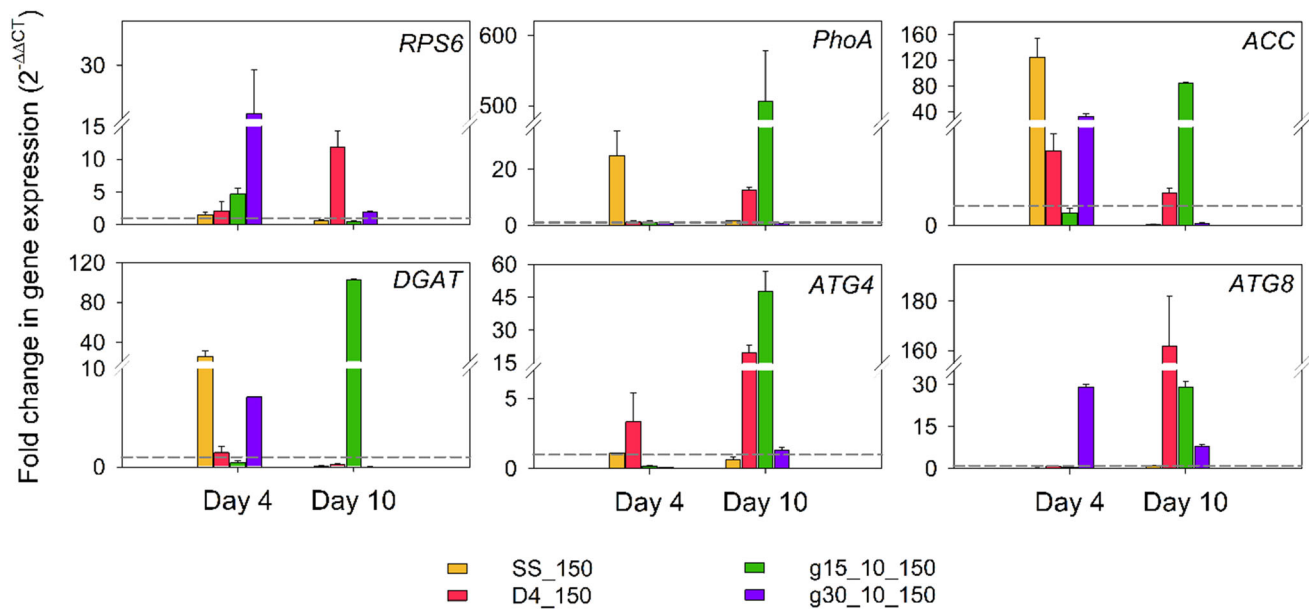
Fig. 12 Fold change in expression of genes affecting the growth, autophagy, and de novo lipid synthesis in *C. reinhardtii* under salt stress. Fold change ($2^{-\Delta\Delta C_T}$) in gene expression was calculated keeping the autotrophy control as the reference, represented by a gray-colored dashed line at fold change = 1. RACK1 is the internal control. *DGAT* Diacylglycerol acyltransferase, *ACC* Acetyl-CoA carboxylase, *PhoA* Starch phosphorylase A, *ATG4* autophagy-related protein ATG4, *ATG8* autophagy-related protein ATG8, *RPS6* ribosomal protein subunit. Day 4 represents the log phase and day 10 represents the stationary phase of the culture

4 Discussion

While salt stress has been extensively studied for improving biofuel production in microalgae, this study provides unique insights into the lipid production of freshwater microalga, *C. reinhardtii* CC-125, at different salt concentrations and modes of cultivation implemented to improve the biofuel and nutraceutical applications. Salt stress beyond a threshold is often fatal to cell survival and sub-lethal effects on the growth and biomolecule accumulation is dose dependent. We found that 150 mM NaCl was the ideal concentration to build an optimum biomass density. Among the NaCl ranging from 25 to 100 mM NaCl in *C. mexicana*, the highest biomass was observed at 25 mM NaCl [28]. The marginal change in the viability of *C. reinhardtii* when the NaCl concentration varied between 50 and 150 mM was also observed in the other studies [29, 30]. Changing the mode of cultivation often aids in an improvement in biomass productivity. In this context, the gradient strategy yielded the maximum biomass at 150 mM NaCl (g30_10_150 with a step size of 2 days boosts the cell density by ~ 1.5 times) and also rescued the cells from dying. The gradient strategy of adding 200 mM NaCl in steps of 2 days resulted in a similar ~ 1.5 times increase in biomass productivity despite a reduced growth rate in *C. reinhardtii*, cultivated under continuous illumination with the light intensity of 81 µmol photons/m² s, higher than the current study [31]. The excess light intensity does not seem to change biomass productivity in gradient cultivation under salt stress.

Increased salinity imposes an osmotic shock on microalgal cells, causing cell size reduction and the formation of palmelloids for protection [1]. Fan et al. [32] show that 0–50 mM NaCl results in efficient photosynthesis in *C. reinhardtii*, but photosynthesis is negatively affected by 100–200 mM NaCl. NaCl at 200 mM resulted in cell death, while at 100 mM *Chlamydomonas* cells show deteriorating growth and maximum lipid content is obtained at 50 mM NaCl [28, 32]. Carbon partitioning and starch-to-lipid switching are essential contributors to the enhanced lipid content observed under high salinity [27, 33]. Intracellularly, it also results in oxidative stress and high ROS levels further activate autophagy-driven lipid accumulation [31]. However, prolonged exposure to high ROS levels is often fatal for photosynthesis and cell growth [31]. Carotenoids can quench the ROS molecules and prevent cell damage [34]. Salt stress is also a common practice to increase carotenoid production in microalgae [1, 35]. This is because there is an increase in intracellular oxidative stress causing ROS production [1, 36]. Increased ROS levels induce autophagy and prolonged exposure leads to cell death [37]. To counter-regulate autophagy, carotenoid production increases [38]. Salt toxicity induces excess production of starch and TAG. Starch molecules act as osmo-protectants and help the cells to adapt to osmotic stress induced by salt exposure [39, 40]. Lipids, especially neutral lipids are important for membrane integrity, which is disturbed due to osmotic imbalance caused by salt toxicity [41]. The interconversion from starch to lipid can occur due to starch-to-lipid switching [33, 42]. Starch

production begins early in the metabolic stage followed by the lipids that are synthesized at the later growth stages [31, 43]. 150 mM NaCl is the optimum concentration to yield the maximum of TAG in the present study. Lipids witness the highest change by 2.5-fold in *Scenedesmus* sp. containing 200 mM NaCl in the surroundings [41]. In *Scenedesmus obtusus* XJ-15, two-stage salt stress causes an increase in lipid productivity by 1.8-fold and changes the fatty acid composition [44]. A freshwater microalga, *Chlorella vulgaris*, can produce 2.45 times excess lipids even in the presence of 500 mM NaCl added in two-stage cultivation due to the tolerance to the oxidative stress induced at high salt concentrations [15]. The current study shows maximum lipid accumulation in the gradient cultivation with 150 mM NaCl, which is nearly 2 times higher than the Control (Fig. 2). The present study shows that a combination of salt concentration changes with gradient strategy helps in enhancing the lipid content in microalgae, without compromising the biomass yield.

An increase in the oxidative levels of the cell under salt toxicity results in enhanced autophagy [45]. Increased ATG8 levels accompanied by enhanced DGAT levels in light-stressed cultures of *C. reinhardtii* results in enhanced TAG accumulation [46]. Autophagy increases lipid production in Haematococcus lacustris under salinity stress [47]. De novo production pathways like fatty acid biosynthesis and TAG synthesis further complement the higher levels of TAG in salt stress in microalgae [48, 49]. An increase in the starch degradation activity is also known to increase the carbon flow towards lipid production and result in starch-to-lipid switching [50]. We observed highly upregulated levels of both catabolic and anabolic pathways in the gradient strategy, i.e., ATG4, ATG8, PhoA, ACC, and DGAT representing autophagy, starch degradation, and de novo lipid synthesis, respectively. These together contribute to the higher levels of observed TAG. In single-stage cultivation, the autophagy levels are low, and the de novo pathway alone is responsible for the lipid content. Two-stage salt stress exhibits autophagy along with protein turnover. However, the downregulation of RPS6 is related to the activation of autophagy [24]. This is the first study to display the varying effect of the mode of cultivation on metabolic pathways and metabolite production.

However, high salinity exerts morphological changes such as palmelloid formation, flagellar resorption, and a decrease in cell size [29]. In *C. reinhardtii*, palmelloid formation starts beyond 50 mM NaCl [51]. Palmelloids protect the cells enclosed within the exopolysaccharide (EPS) matrix from further external damage [52]. This study, for the first time, provides a detailed analysis of changing cell morphology as a function of the mode of cultivation. Single-stage cultivation with 150 mM NaCl exhibits palmelloid formation, otherwise insignificant or delayed in two-stage and gradient cultivations. 2–4 celled structures were observed in *C. reinhardtii* strain GY-D55 containing a higher salt concentration of 300 mM [53]. Osmotic shock results in size reduction but intact circularity in the single-stage cells with 150 mM NaCl. The gradient cultivation, g30_10_150, with maximum biomass content shows small change in their cell size. Bimodal distribution appears in two-stage cultivations signifying the development of stress-combat strategies in the population. These sub-populations slowly grow and take over the existing cells in the population, giving way to evolution for survival [54, 55].

The TAG molecules synthesized under stress are enclosed by a phospholipid monolayer when pinched off from the endoplasmic reticulum (ER) membrane [10], which form lipid droplets (LD). The nucleation and growth of the lipid droplets is strongly influenced by the mechanical properties of the ER membrane, which lead to a difference in the nucleation energy barrier, with ER tubule observed to produce smaller droplets compared to the ER sheet [56]. The phospholipid saturation increases rigidity, thereby increasing the cost of the deformation energy for curvature to produce droplets. The chemical composition of the neutral lipids produced influences the chemical potential for phase separation [56]. Moreover, the protein seipin has been observed to play a major role in the nucleation of lipid droplets [56]. In the present case, the size distribution of LDs is observed to differ with the mode of cultivation, with enhancement in LD size on increasing the salt concentration. The LD size is believed to be governed by the physical phenomena of Ostwald ripening or droplet coalescence [9, 10]. The protein seipin in the outer layer of LDs and DGAT, involved in TAG synthesis, has also been shown to regulate the size of LD [5]. The major lipid droplet proteins (MLDP) present in the outer layer of droplets in *C. reinhardtii* and *Phaeodactylum tricornutum* have been revealed to regulate the droplet size without affecting their metabolism and composition [57, 58]. The chain length of fatty acids and unsaturation content present in triacylglycerols also modulate the size of LDs [59, 60]. Since the fatty acid composition is likely to change with the environmental condition [61, 62], the LD growth dynamics can vary as a result under different modes of cultivation under salt stress. The degradation of LDs to release energy when required to carry out metabolic activities also influences the LD size, and in this condition, the size and number of LDs become independent of the actual concentration of the neutral lipid molecules [12]. The gradient cultivation is the perfect example where the lipid content is high but the number of LDs is low (Figs. 2 and 7), with predominantly larger-sized lipid droplets. Lipid droplet biogenesis begins with initial phase separation or demixing in the ER membrane [6]. The droplet formation by liquid–liquid phase separation (LLPS) theory can be described by generalizing the Flory–Huggins relation for free energy [63], originally developed for polymer solutions, given by Eq. (1):

$$F = (1 - \varphi) \ln(1 - \varphi) + \frac{1}{M} \varphi \ln \varphi + \in \varphi(1 - \varphi) \tag{1}$$

where the lipid volume fraction is given by φ, M is the molecular weight of the lipid, and $\in$ is the interaction energy term, involving the phospholipids at the interface, given by $\in = -zw/2k_BT$, where z is the coordination number, k_B is the Boltzmann constant, and $w = e_{LL} + e_{CC} - 2e_{SCL}$. e_{SCL} is the interaction energy term arising due to the interfacial phospholipid monolayer, e_{LL} is the interaction energy between the lipid molecules, whereas e_{CC} is the average interaction arising due to the components of the hydrophilic gel-like cytosol. In the presence of interactions not favoring the close proximity of different species, demixing occurs for a certain range of volume fractions. The chemical potential is given by $\mu = \varphi\frac{dF}{d\varphi}$. This chemical potential can be equal for two different compositions, leading to a thermodynamically stable demixed state, and a curved phase boundary, enclosing a range of demixed or phase-separated states, as observed in Fig. 11.

In microalgae, LLPS plays a vital role in sensing oxidative stress and aids LD organization [4]. The presence of an increased two-phase state, explained by the function of area fraction of lipid droplet with culture age, in single stage could be due to the enhanced lipid concentration. The LD biogenesis differs among organelles. The nuclear LDs are different from the cytoplasmic ones [64]. The LD formation is believed to initiate from both ER and chloroplast in microalgae [65]. The spatial differences and membrane bending energy barrier are likely to regulate the phase separation and initial LD size to a great extent [66, 67]. These features of droplet biogenesis would vary under stress [66], because of which the demixed state increases under salt stress. It is, therefore, not surprising that the phase coexistence boundary varies greatly for different modes of growth (Fig. 11), with the single-stage growth having maximum area of demixed phase inside the phase boundary, and D4_150 hinting at a tendency for reentrance of the one-phase region near the 5th day of growth.

5 Conclusions

Summarizing, this study analyzes lipid productivity and LLPS of lipid droplets formed in *C. reinhardtii* strain CC-125 under salt stress. The effects have been monitored at single-cell level for different aspects of growth and production of lipids. Changing the mode of cultivation to gradient from single-stage salt application enhanced biomass and lipid production. Gradient strategy minimizes the negative effects of osmotic stress on cellular morphology. Manner of application of stress modulates the size as well as the chemical nature of the lipid droplets. The phase separation involved in lipid droplet formation under salt stress varies with the mode of cultivation. It depends on the lipid concentration balanced by the synthetic and breakdown pathways. The present study enlightens the relationship between the altering culture settings in presence of salt toxicity and the metabolic description of the microalgal cell. It signifies that the mode of cultivation is a key factor in diverting the metabolite production pathway from starch to lipid or vice versa. LLPS could be the survival strategy adopted by the cells to combat oxidative stress due to high salinity. Effect of salinity stress on lipid droplets is analyzed by exploring various attributes of LLPS such as number, size, or area fraction of lipid droplets, in addition to fluctuations of these parameters and spatial segregation of droplets for different modes of cultivation and culture age. This study is, therefore, significant in order to relate the phenomenon of LLPS to optimized lipid productivity.

Author contributions

SP—conceptualization, experiments and data analysis, manuscript preparation; PV, VP—acquisition of data; JJ—primer designing for RT-PCR, GA—project management, resources; DB—data analysis, manuscript preparation, and project management.

Data availability Data can be obtained from the corresponding author on reasonable request.

Declarations

Conflict of interests The authors have no conflict of interest.

References

1. E. Bazzani, C. Lauritano, O. Mangoni, F. Bolinesi, M. Saggiomo, J. Mar. Sci. Eng. **9**, 1242 (2021)
2. S.H. Ho, A. Nakanishi, X. Ye, J.S. Chang, K. Hara, T. Hasunuma, A. Kondo, Biotechnol. Biofuels **7**, 1 (2014)
3. T. Atikij, Y. Syaputri, H. Iwahashi, T. Praneenararat, S. Sirisattha, H. Kageyama, R. Waditee-Sirisattha, Mar. Drugs **17**, 484 (2019)
4. Y. Saito, W. Kimura, Front. Genet. **12**, 1 (2021)
5. V. Zoni, R. Khaddaj, P. Campomanes, R. Thiam, R. Schneiter, S. Vanni, SSRN Electron. J. **1**, 137 (2020)
6. J.A. Olzmann, P. Carvalho, Nat. Rev. Mol. Cell Biol. **20**, 137 (2019)
7. L.V. Chernomordik, M.M. Kozlov, Annu. Rev. Biochem. **72**, 175 (2003)
8. A.R. Thiam, B. Antonny, J. Wang, J. Delacotte, F. Wilfling, T.C. Walther, R. Beck, J.E. Rothman, F. Pincet, Proc. Natl. Acad. Sci. U. S. A. **110**, 13244 (2013)
9. D. Georgieva, V. Schmitt, F. Leal-Calderon, D. Langevin, Langmuir **25**, 5565 (2009)
10. T.C. Walther, J. Chung, R.V. Farese, Annu. Rev. Cell Dev. Biol. **33**, 491 (2017)
11. A.R. Thiam, L. Forêt, Biochim. Biophys. Acta Mol. Cell Biol. Lipids **1861**, 715 (2016)
12. J. Yu, P. Li, Sci. China Life Sci. **60**, 46 (2017)
13. S. Nagappan, S. Devendran, P.C. Tsai, H.U. Dahms, V.K. Ponnusamy, Fuel **252**, 339 (2019)
14. I. Pancha, K. Chokshi, R. Maurya, K. Trivedi, S.K. Patidar, A. Ghosh, S. Mishra, Bioresour. Technol. **189**, 341 (2015)
15. C.J. Yun, K.O. Hwang, S.S. Han, H.G. Ri, Biomass Bioenergy **127**, 105277 (2019)
16. W. Maneechote, B. Cheirsilp, Bioresour. Technol. **328**, 124850 (2021)
17. Y. Xie, K. Lu, X. Zhao, R. Ma, J. Chen, S.H. Ho, Biotechnol. J. **14**, 1 (2019)
18. P. Zhang, Z. Li, L. Lu, Y. Xiao, J. Liu, J. Guo, F. Fang, Spectrochim. Acta A Mol. Biomol. Spectrosc. **181**, 30 (2017)
19. R.S. Gour, V.K. Garlapati, A. Kant, Curr. Microbiol. **77**, 779 (2020)
20. W. Chen, C. Zhang, L. Song, M. Sommerfeld, Q. Hu, J. Microbiol. Methods **77**, 41 (2009)
21. Z. Kou, S. Bei, J. Sun, J. Pan, J. Appl. Phycol. **25**, 1633 (2013)
22. S. A. Bell, C. Shen, A. Brown, A. G. Hunt, PLoS One **11**(1), e0146107 (2016)
23. H. Lv, G. Qu, X. Qi, L. Lu, C. Tian, Y. Ma, Genomics **101**, 229 (2013)
24. M. Pérez-Pérez, I. Couso, L. Heredia-Martínez, J. Crespo, Cells **6**, 36 (2017)
25. Y. Li-Beisson, F. Beisson, W. Riekhof, Plant J. **82**, 504 (2015)
26. X. Johnson, J. Alric, Eukaryot. Cell **12**, 776 (2013)
27. S.H. Ho, A. Nakanishi, Y. Kato, H. Yamasaki, J.S. Chang, N. Misawa, Y. Hirose, J. Minagawa, T. Hasunuma, A. Kondo, Sci. Rep. **7**, 1 (2017)
28. E.S. Salama, H.C. Kim, R.A.I. Abou-Shanab, M.K. Ji, Y.K. Oh, S.H. Kim, B.H. Jeon, Bioprocess Biosyst. Eng. **36**, 827 (2013)
29. D.K. Khona, S.M. Shirolikar, K.K. Gawde, E. Hom, M.A. Deodhar, J.S. D'Souza, Algal Res. **16**, 434 (2016)
30. G. Mastrobuoni, S. Irgang, M. Pietzke, H.E. Aßmus, M. Wenzel, W.X. Schulze, S. Kempa, BMC Genom. **13**, 1 (2012)
31. S. Fal, A. Aasfar, R. Rabie, A. Smouni, H. EL Arroussi, Heliyon **8**, 8811 (2022)
32. J. Fan, I. Zheng, J. Biosci. Bioeng. **124**, 302 (2017)
33. L. Zhang, H. Pei, S. Chen, L. Jiang, Q. Hou, Z. Yang, Z. Yu, Bioresour. Technol. **250**, 449 (2018)
34. M.E. Pérez-Pérez, I. Couso, J.L. Crespo, Autophagy **8**, 376 (2012)
35. J.R. Benavente-Valdés, C. Aguilar, J.C. Contreras-Esquivel, A. Méndez-Zavala, J. Montañez, Biotechnol. Rep. **10**, 117 (2016)
36. K. Chokshi, I. Pancha, A. Ghosh, S. Mishra, Bioresour. Technol. **244**, 1376 (2017)
37. M.J. Affenzeller, A. Darehshouri, A. Andosch, C. Lütz, U. Lütz-Meindl, J. Exp. Bot. **60**, 939 (2009)
38. Y. Ren, H. Sun, J. Deng, J. Huang, F. Chen, Mar. Drugs **19**, 713 (2021)
39. Z. Tietel, W.R. Wikoff, T. Kind, Y. Ma, O. Fiehn, Eur. J. Phycol. **55**, 11 (2020)
40. P.R. Pandit, M.H. Fulekar, M.S.L. Karuna, Environ. Sci. Pollut. Res. **24**, 13437 (2017)
41. X. Ji, J. Cheng, D. Gong, X. Zhao, Y. Qi, Y. Su, W. Ma, Sci. Total. Environ. **633**, 593 (2018)
42. Y. Kato, S.H. Ho, C.J. Vavricka, J.S. Chang, T. Hasunuma, A. Kondo, Bioresour. Technol. **245**, 1484 (2017)
43. L.T. Hang, K. Mori, Y. Tanaka, M. Morikawa, T. Toyama, Bioprocess Biosyst. Eng. **43**, 971 (2020)
44. L. Xia, H. Ge, X. Zhou, D. Zhang, C. Hu, Bioresour. Technol. **144**, 261 (2013)
45. M.J. Affenzeller, A. Darehshouri, A. Andosch, C. Lutz, U. Lutz-Meindl, J. Exp. Bot. **60**, 939 (2009)
46. N. Chouhan, E. Devadasu, R.M. Yadav, R. Subramanyam, Front. Plant Sci. **12**, 789 (2022)
47. D.A. Zharova, A.N. Ivanova, I.V. Drozdova, A.I. Belyaeva, O.N. Boldina, O.V. Voitsekhovskaja, E.V. Tyutereva, Plants **11**, 197 (2022)
48. M. Iwai, K. Ikeda, M. Shimojima, H. Ohta, Plant Biotechnol. J. **12**, 808 (2014)
49. R. Rengel, R.T. Smith, R.P. Haslam, O. Sayanova, M. Vila, R. León, Algal Res. **31**, 183 (2018)
50. Y. Kato, T. Oyama, K. Inokuma, C.J. Vavricka, M. Matsuda, R. Hidese, K. Satoh, Y. Oono, J.-S. Chang, T. Hasunuma, A. Kondo, Commun. Biol. **4**, 450 (2021)
51. S. Neelam, R. Subramanyam, J. Photochem. Photobiol. B. **124**, 63 (2013)
52. P. Shetty, M.M. Gitau, G. Maróti, Cells **8**, 1 (2019)
53. L.Y. Zhang, Z.T. Xing, L.Q. Chen, X.J. Zhang, S.J. Fan, Front. Plant Sci. **13**, 1 (2022)
54. S.J. Altschuler, L.F. Wu, Cell **141**, 559 (2010)

55. M.E. Lidstrom, M.C. Konopka, Nat. Chem. Biol. **6**, 705 (2010)
56. A.R. Thiam, E. Ikonen, Trends Cell Biol. **31**, 108 (2021)
57. E.R. Moellering, C. Benning, Eukaryot. Cell **9**, 97 (2010)
58. X. Wang, T. Bin-Hao, S. Balamurugan, W.D. Yang, J.S. Liu, H.P. Dong, H.Y. Li, Algal Res. **26**, 215 (2017)
59. S.H. Son, G. Park, J. Lim, C.Y. Son, S.S. Oh, J.Y. Lee, Nat. Commun. **13**, 1 (2022)
60. M. Lange, P.V. Wagner, M. Fedorova, Free Radic. Res. **55**, 469 (2021)
61. B.R. Moser, In Vitro Cell Dev. Biol. Plant **45**, 229 (2009)
62. W. Yu, W. Ansari, N.G. Schoepp, M.J. Hannon, S.P. Mayfield, M.D. Burkart, Microb. Cell Fact. **10**, 1 (2011)
63. P.J. Flory, in *Principles of Polymer Chemistry*, ed. by P.J. Flory (Cornell Univ. Press, New York, 1953), p. 688
64. T. Fujimoto, J. Cell Sci. **135**, 5 (2022)
65. H. Goold, F. Beisson, G. Peltier, Y. Li-Beisson, Plant Cell Rep. **34**, 545 (2015)
66. V. Zoni, R. Khaddaj, P. Campomanes, A.R. Thiam, R. Schneiter, S. Vanni, Elife **10**, 1 (2021)
67. J. Mahamid, D. Tegunov, A. Maiser, J. Arnold, H. Leonhardt, J.M. Plitzko, W. Baumeister, Proc. Natl. Acad. Sci. U. S. A. **116**, 16866 (2019)